

Article

Unique Interstitial Textures within Coarse-Grained Jadeitite from Kazakhstan and Their Significance in Locality Identification

Jiabao Wen ¹, Guanghai Shi ^{1,*} , Biqian Xing ¹, Taafee Long ² and Jinhong Zhang ³¹ School of Gemmology, China University of Geosciences (Beijing), Beijing 100083, China² Guangdong Gemstones & Precious Metals Testing Center, Guangzhou 510080, China³ The World of Jade Museum & Exhibition Centre, Sihui 526200, China

* Correspondence: shigh@cugb.edu.cn

Abstract: Unique finer-grained interstitial textures, occurring as small blocks or irregular shapes of 0.15–10 mm, were found merging in the coarse-grained textures of Kazakhstan jadeitite. According to the mineral content, the interstitial texture could be classified into two types: Type I, consisting of almost all jadeite crystals, minor omphacite, and little analcime, and Type II, comprising mainly omphacite and analcime, with minor jadeite crystals. They both showed no obvious preferred orientation and have distinct boundaries with the coarse-grained textures but appear more transparent, with finer grain sizes and higher degrees of idiomorphism. The coarse-grained textures include granitoid textures and radial clusters. The granitoid textures formed by euhedral to subhedral prismatic grains usually show rhythmic zoning patterns and parallel intergrowths. Furthermore, fluid inclusions contain H₂O and CH₄, and it was supposed that the coarse-grained textures were formed by the precipitation of jadeitic fluids. However, perhaps due to the insufficient supply of the fluids or sufficient space, some interspaces were left among the coarser-grained jadeitite. Afterward, these interspaces were filled with precipitation of the successor H₂O-richer fluids under a different P–T condition from that of the former coarser-grained jadeitite, and consequently, two kinds of interstitial textures formed. Such interstitial textures seem to appear only in Kazakhstan and therefore could serve as a typical visual identification feature of Kazakhstan jadeitite.

Keywords: Kazakhstan; jadeitite; microstructure; coarse-grained texture; interstitial texture



Citation: Wen, J.; Shi, G.; Xing, B.; Long, T.; Zhang, J. Unique Interstitial Textures within Coarse-Grained Jadeitite from Kazakhstan and Their Significance in Locality Identification. *Minerals* **2023**, *13*, 513. <https://doi.org/10.3390/min13040513>

Academic Editor: Panagiotis Voudouris

Received: 1 March 2023

Revised: 28 March 2023

Accepted: 2 April 2023

Published: 4 April 2023



Copyright: © 2023 by the authors. Licensee MDPI, Basel, Switzerland. This article is an open access article distributed under the terms and conditions of the Creative Commons Attribution (CC BY) license (<https://creativecommons.org/licenses/by/4.0/>).

1. Introduction

Jadeitite, a rock composed almost entirely of jadeite and related pyroxenes, is found in the serpentinite mélange and is associated with high-pressure and low-temperature metamorphic rocks such as eclogite and blueschist. It is rare worldwide and found only at ~19 locations distributed in the Caribbean orogenic belt, Alpine–Himalayan orogenic belt, Caledonia orogenic belt, and Circum Pacific orogenic belt, including the southern and northern Motagua Fault Zone in Guatemala [1–3], Cuba [4], Dominica [5], Japan (Itoigawa–Omi [6], Osayama [7], Oya–Wakasa [8], Nishisonogi [9], Kamuikotan Gorge area [10], America (New Idria [11]; Ward Creek [12]), Papua New Guinea [13], Greece [14], Italy [15], Iran [16], Myanmar [17,18], Russia [19], and Kazakhstan (Kenterlau–Itmurunda–Arkarsu) [20]. However, due to its scientific significance and commercial importance, jadeitite has always attracted the attention of geologists, gemologists, mineral enthusiasts, and jewelry consumers. Tsujimori and Harlow (2012) categorized jadeitite genesis into two types: P-type (precipitation) and R-type (replacement) [21,22]: Na–Al–Si-rich fluids can precipitate in serpentinitized peridotite fractures or low-temperature, high-pressure metamorphic rocks; do not exhibit characteristics of protolithic rocks or minerals; or alternatively, replace protolith such as plagiogranite and metagabbro to generate jadeite, with visible protolith textures [1,23–26]. Rhythmical zoning patterns, euhedral to subhedral prismatic

textures, and fluid inclusions commonly occur in the P-type jadeitite [27], while the R-type can show evidence of the replacement of precursor rocks [21]. Jadeitite recrystallizes as a result of dynamic metamorphism, forming varying degrees of deformed textures. This process has a positive influence on the compositional homogeneity, and reduction in the grain size of the jadeite aggregate and a significant number of recovery textures, such as serrated high-angle sutured boundaries and fine grains with a high degree of preferred orientation, can be seen in icy and glassy jadeitite from Myanmar [27,28]. Following the formation of jadeitite, the application and withdrawal of various stresses, as well as the lowering of temperature, can result in rock cracks. The fluids then flow in and crystallize, forming filling textures such as comb-like structures and jadeite veinlets [27]. Such observations of jadeitite microstructures, which are closely related to features visible to the unaided eye, have some implications for genetic studies and the determination of its locality.

In this work, partial jadeitite domains with unique finer interstitial textures within coarse jadeitite from Kazakhstan are found and scrutinized. This kind of texture, enhancing the partial transparency, might have potential implications for genetic studies and distinguishing the Kazakhstan jadeitite from that of other localities.

2. Geological Setting

Kazakhstan jadeitite is found in Karaganda, where it meets Early to Middle Ordovician pelagic sediments. The Kazakhstan plate is a part of the Central Asian orogenic belt, which was produced by subduction as well as reduction in the Paleo-Asian Ocean [29]. The microcontinents and island arcs are divided by suture zones that consist of Neoproterozoic to Early Silurian deep, marine, volcanic, sedimentary formations and ophiolites [29,30], and the microcontinents are primarily Paleoproterozoic basement and Neoproterozoic to Early Paleozoic cover [30]. In the Late Silurian, the Kazakhstan plate was collaged into a composite arc [30–33] (Figure 1). The Kazakhstan jadeitite deposit formed in the Early Paleozoic Junggar Balkhash fold system at ~450 Ma and is one of the world's oldest jadeitite occurrences [21,34,35] (Figure 1). The studied deposit occurs as inclusions in Chuerkulam's shattered and schistositized serpentinite mélangé near Balkhash Lake. Sorensen et al. (2006) discovered a massive amount of compositional zoning patterns in Kazakh jadeitite via cathodoluminescence (CL), indicating that the jadeitite is primarily of P-type origin [36]. The most typical mineral assemblage in this location is jadeite + albite + analcime + omphacite, which can be found in block and water drop shapes with varying degrees of albitization. The blackwall is located at the boundary between jadeitite and serpentinite, which is composed of chlorite and actinolite [37–41].

The classic occurrence of Kazakhstan jadeitite was detailed and introduced by Harlow and Sorensen (2005) [37]. Three different jadeitite rock types can be seen in this area (Figure 2): (1) white jadeitite rock can be seen in the middle of the rock block; (2) colored jadeitite with albite; and (3) altered (dark green) jadeitite rock: the edge of the jadeitite rock was altered and may contain mica, garnet, and other minerals [37].

Commercially, the majority of the jadeitite in this region is generally coarse-grained, usually white, gray, or lavender, and the ground exhibits a porcelain-like luster and coarse-grained textures at a size of 0.2–4.0 mm. Omphacite in dark green occurs as veins. Vivid green jadeitite can be seen in patches and veins between the omphacite and porcelain-white jadeitite. The jadeitite from Kazakhstan also exhibits a weathered yellow hue, similar to that from Myanmar [42].

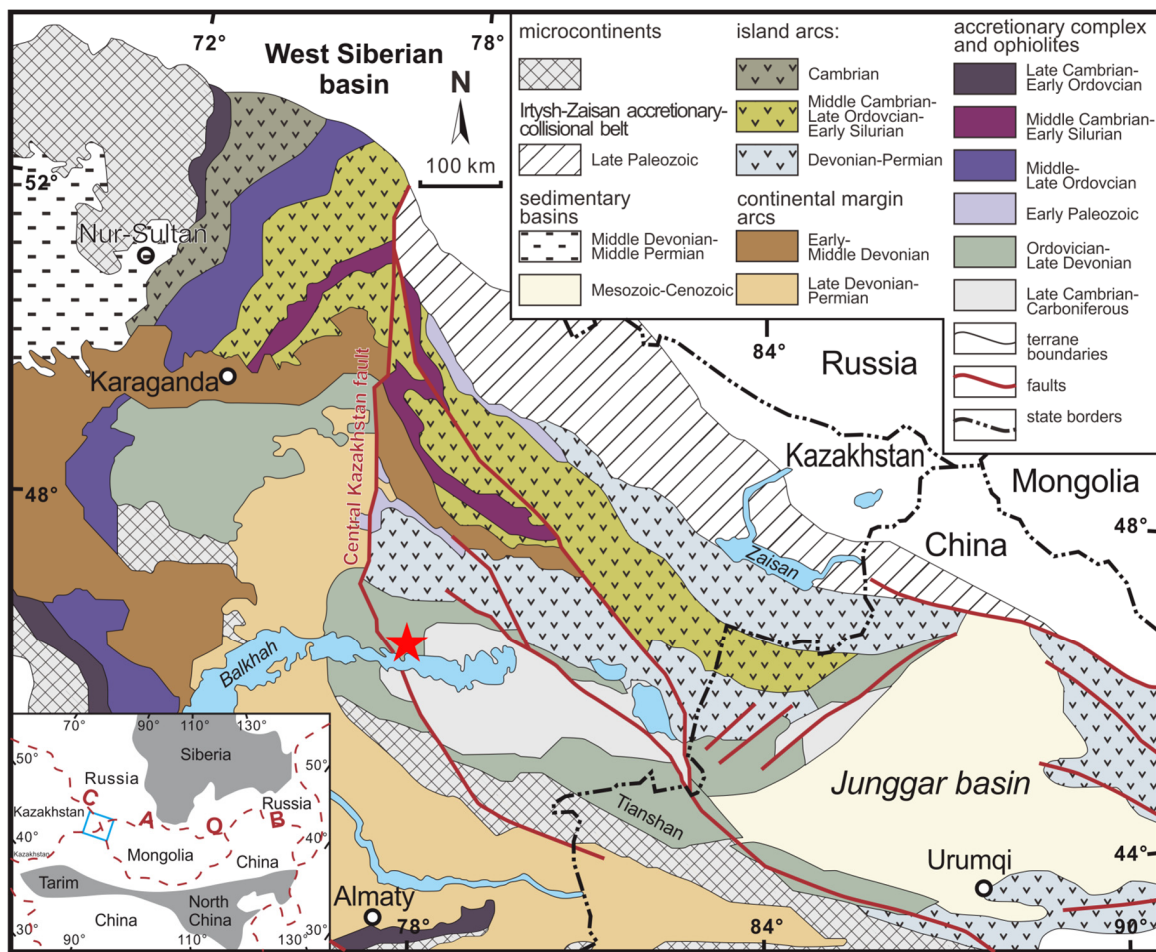


Figure 1. Simplified tectonic scheme of the western Central Asian Orogenic Belt and location of the Itmurundy belt shown as red star (Adapted with permission from Refs. [31,40], Copyright (2023), with permission from Elsevier).

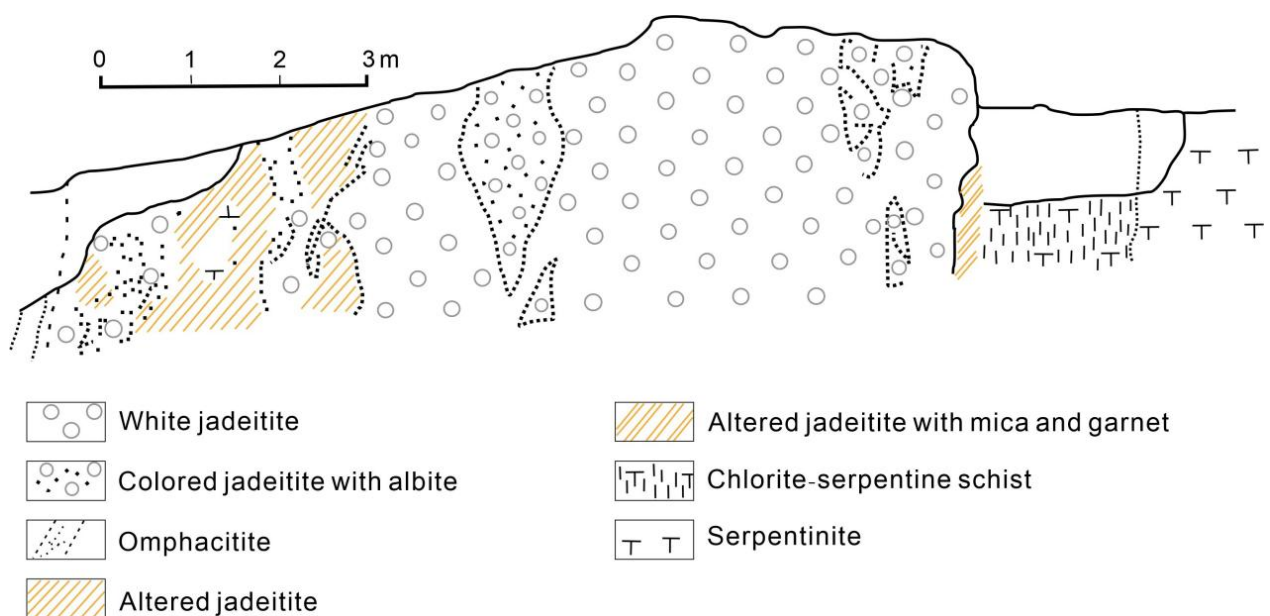


Figure 2. Cross section of Kazakhstan jadeitite in ultramafic rock mass (modified from [37,43]).

3. Materials and Methods

In this article, 19 polished samples from Kazakhstan, handed over by a local mine owner to 1 coauthor, JHZ, were observed and found to have a number of much more transparent domains (MTDs) with distinctive, angular borders included within the coarser-grained jadeitite. These MTDs can reach ~20 mm and occur separately in light green jadeitite or, randomly, porcelain-white jadeitite. These domains are finer-grained, more compact and thus graded as higher quality. In order to characterize this observation, two representative samples (labeled K01 and K02) were selected for petrographic and gemological studies (Figure 3).

Raman spectroscopy (Horiba HR Evolution confocal laser Raman spectrometer) and specific gravity analysis, which was measured using the hydrostatic weighting method, were performed in the Experimental Teaching Center of Gemmology, School of Gemmology, China University of Geosciences, Beijing (CUGB). The Raman spectrometric analysis (laser beam diameter: ~2 μm) was performed using a 532 nm laser source, 100 μm slit width, 600 gr/mm grating, 3 s scanning time, integration number = 1–3, and a collection range of 200–4000 cm^{-1} . Optical observation was observed using an OLYMPUS BX53 polarizing microscope. The cathodoluminescence photos and polarized photos were taken at Resources Exploration Laboratory, CUGB, using a cathodoluminescence meter under 13–15 kV, 250 μA , and 0.003 bar. An electron probe instrument test and BSE images acquisition were done at the Institute of Minerals Resources, Chinese Academy of Geological Sciences using a JXA-8230 electronic probe microanalyzer under the conditions of acceleration voltage 15 KV, current 10 nA, electron beam diameter less than 10 μm , and using the ZAF correction procedure. The standard samples were determined from the following minerals: andradite (Si and Ca), rutile (Ti), corundum (Al), hematite (Fe), chromite (Cr), rhodonite (Mn), nickel (Ni), magnesia (Mg), albite (K), and barite (Ba) measures.

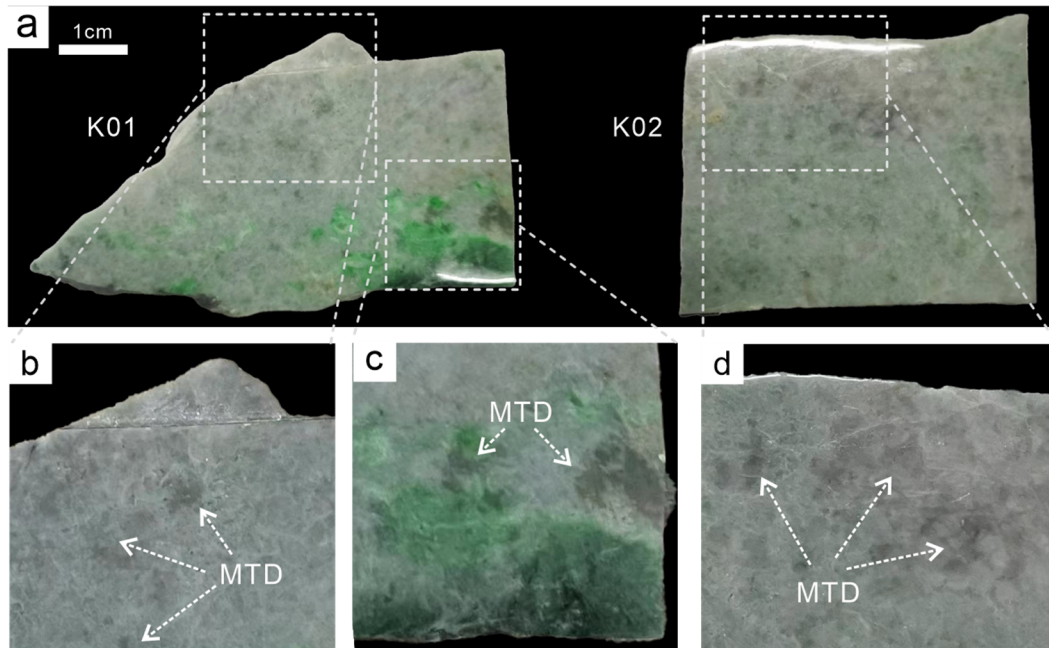


Figure 3. (a) Photos of the studied samples: smaller-grained, more transparent domains (MTDs) could be observed among the coarser-grained basement of the polished samples. (b–d) Local magnification of several MTDs in (a).

4. Results

Using still-water weight measurement, the specific gravity of the two samples was 3.23, which is slightly lighter than that of jadeitite from Myanmar [27].

4.1. Texture/Microstructure of Coarser-Grained Jadeitite

The coarser-grained jadeitites display granitoid or mosaic textures with parallel intergrowths and rhythmic zoning patterns (Figures 4 and 5). In granitoid textures, the jadeites (Jd-I) are typically prismatic and radial (with a length of 0.2–4 mm), with the majority being euhedral or subhedral with cleavages. The grain boundaries are flat. Under cross-polarized light, parallel intergrowths exhibit nearly identical interference colors and extinction positions between two single crystals.



Figure 4. The jadeite grains display euhedral to subhedral prismatic crystal habits (under cross-polarized light).

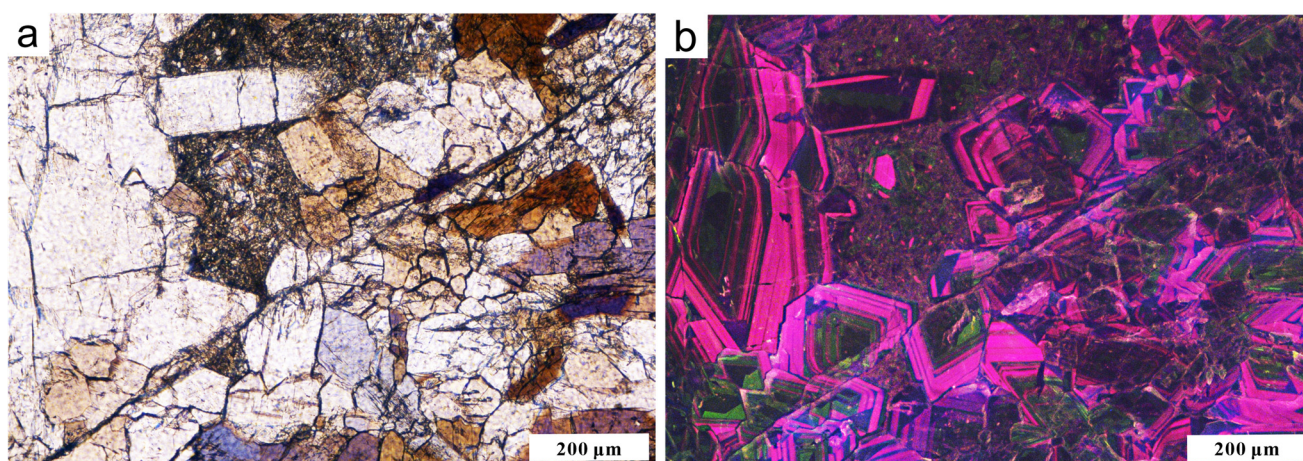


Figure 5. Rhythmic zoning patterns (RZPs). (a) Photo under cross-polarized light. (b) The same parts show clear RZPs under cathodoluminescence.

The rhythmical zoning patterns of coarser-grained jadeite crystals are visible under cathodoluminescence. The jadeite grains contain 5 to 15 or even more bands. Zoned jadeites often have dark green layers and inert areas at the cores, with alternating brilliant pink and inert layers around the cores. Each layer ranges from 5 to 30 μm in size (Figure 5). The rhythmic zoning patterns indicate a P-type origin for jadeite formation [18,22,27].

There are fluid inclusions in jadeite grains that are approximately 3–20 μm long. Gaseous bubbles can also be observed. The inclusions are primary and mostly elongated along the c-axis of the jadeites (Figure 6a).

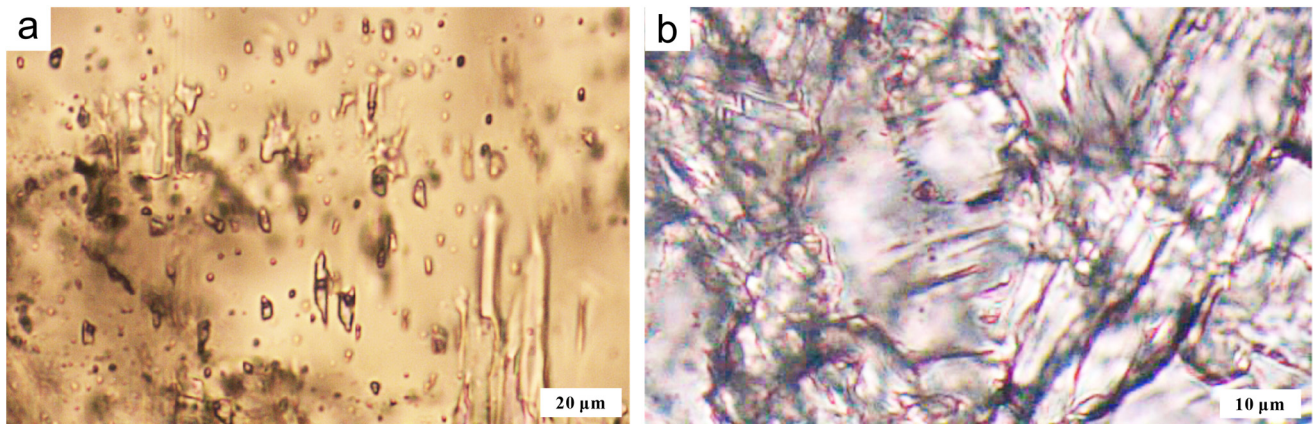


Figure 6. (a) Fluid inclusions in coarser-grained jadeites. (b) Fluid inclusions in Type I filling jadeite.

4.2. Texture/Microstructure of More Transparent Domains (MTDs)

The more transparent domains fill the interspaces of the coarser-grained jadeite and are outlined by large, flat jadeite grains. As their grains are much finer than those of the host jadeite aggregate, it is easy to distinguish them. According to mineral content, the domains can be categorized into two types: jadeite-dominated domains (Type I) and jadeite–omphacite–analcime domains (Type II).

Type I MTDs consists predominately of jadeite crystals (~90 vol.%), with minor omphacite (~9 vol.%) and analcime (~1 vol.%). The jadeite in Type I MTDs is subhedral to anhedral prismatic with a length of 0.02–0.10 mm, occupying the interspaces within the coarser-grained jadeite hosts. The filling jadeite grains do not show a preferred orientation. Some grains have boundaries with 120° quasi-triple junctions (Figure 7a). The filling phases in the domains have green CL luminescence, in contrast to the inert and bright pink luminescence of the coarser host grains (Figure 7b). Some fragments from coarser grains with visible bright pink CL luminescence occur among the finer aggregates with green CL luminescence. The omphacites in the domains are anhedral and occur around the finer-grained jadeites (Figure 7c). Fluid inclusions with sizes of ~5 μm can also be found (Figure 6b).

Type II MTDs contains jadeite (~30 vol.%), omphacite (~40 vol.%), and analcime (~30 vol.%). The composed mineral grains are smaller than 0.05 mm in size and are randomly oriented. Jadeite and omphacite occur as euhedral prisms, and some of the omphacite is found around the jadeite. Analcime occurs as anhedral fillings in the interspaces among finer pyroxenes (Figure 8), showing a formation sequence from jadeite to omphacite to analcime.

Under CL images, the filled grains appear as multiple-layer zonings, with the majority of the bands being bright pink to blueish purple, thin, and straight. The cores of the coarser grains appear inert. The dark purple luminescent filling phase is interspersed with several finer grains (green CL luminescence) in the interspaces (Figure 8b). It is difficult to find fluid inclusions in Type II grains because of their tiny size.

In both types of MTDs, many host jadeite crystals have overgrowths with wide widths from 5.0 to 65 μm across (Figures 7c and 8c). The overgrowths appear similar in brightness to the filling jadeite under the BSE images and grow along the outlines of host crystal clusters.

Type I and Type II domains can be present in the same coarser-grained jadeite interspace (Figure 9). The grains in Type I domains are much larger than those in Type II. In addition, the obvious cataclasis can be observed in coarse grains of the whole thin section.

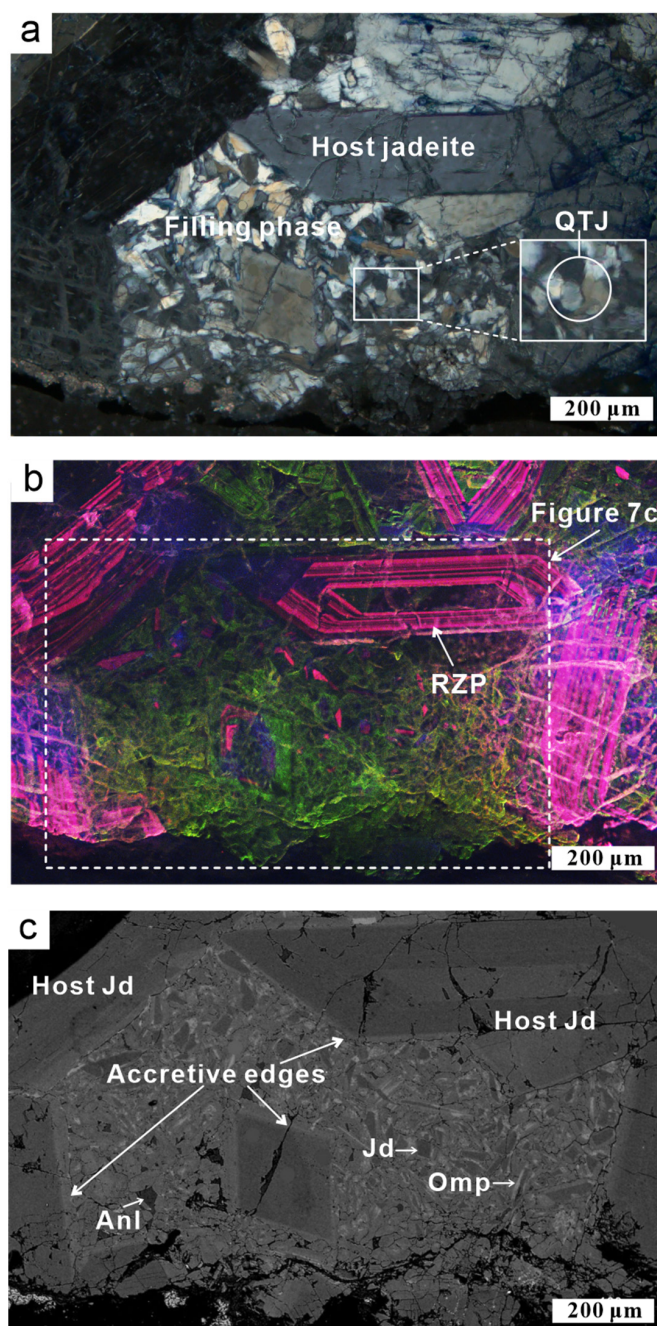


Figure 7. (a) In Type I MTDs, the interspace is filled with subhedral jadeite grains, showing high degree of compactness. (b) Cathodoluminescence picture of (a), the rhythmic zoning patterns (RZPs) visible in the coarser grains. (c) BSE image of (a) shows clearly overgrowths on the outlines of coarser grains and the relationship between the filling jadeite, omphacite, and analcime in Type I interstitial textures (Jd—Jadeite, Omp—Omphacite, and Anl—Analcime).

4.3. Raman Spectra and Chemical Compositions of Minerals

The minerals in the interstitial textures were tested using Raman spectroscopy. The host jadeite shows very strong Raman peaks at 200, 287, 371, 505, 696, 984, and 1035 cm^{-1} , and the peaks of jadeite in MTDs are at 144, 202, 254, 373, 431, 573, 699, 987, and 1038 cm^{-1} . Peaks at ~ 1110 and 1606 cm^{-1} of analcime also exist (Figure 10a). Analcime shows distinct peaks at 299, 381, 484, 637, 821, 1110, 1184, 1229, 1295, 1462, 1606, and 3548 cm^{-1} (Figure 10b); omphacite shows prominent Raman peaks at 272, 301, 339, 374, 682, 823, and

1015 cm^{-1} , with analcime peaks at 484, 1110, and 1606 cm^{-1} (Figure 10c). CH_4 (gas) and H_2O (liquid) in the fluid inclusions of jadeite are detected (Figure 10d).

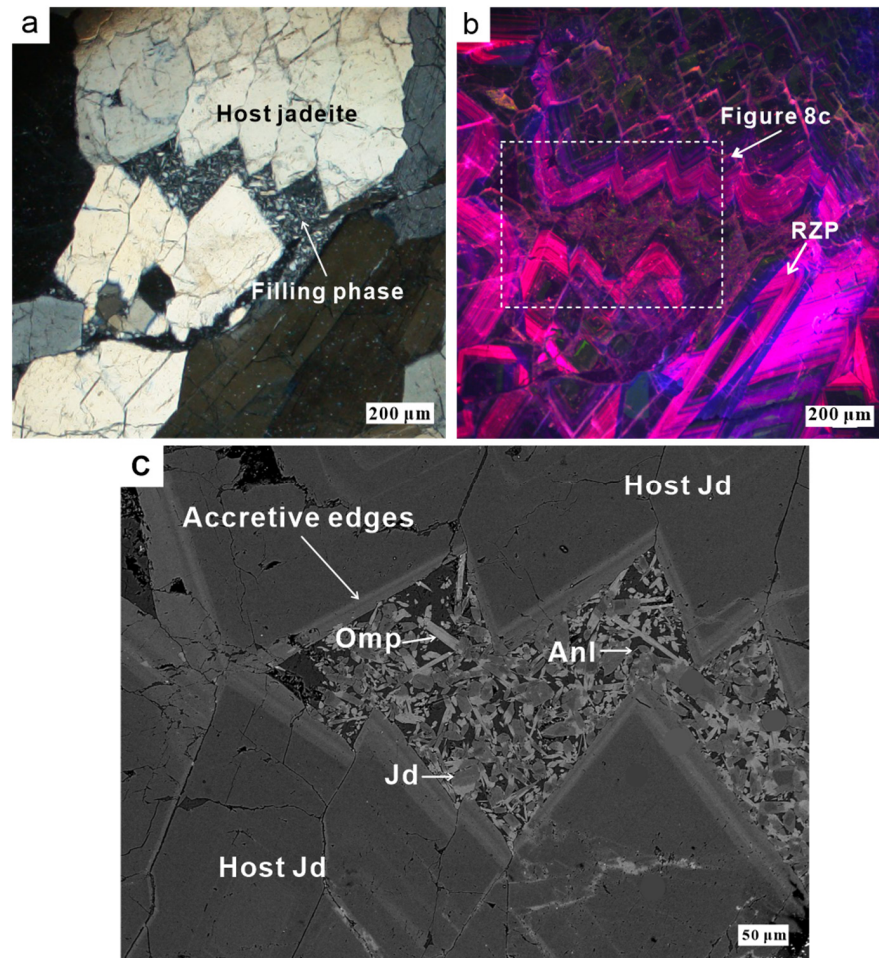


Figure 8. (a) In Type II MTDs, the surrounding host grains show mainly primary texture in which dynamic metamorphism and recrystallization cannot be observed with 10 \times magnification under cross-polarized light. (b) The cathodoluminescence picture of (a) shows visible rhythmic zoning patterns inside the host grains. (c) The BSE image of the part of (a) shows clearly overgrowths on the outlines of host grains and the relationship between the filling jadeite, omphacite, and analcime in Type II interstitial textures (Jd—Jadeite, Omp—Omphacite, and Anl—Analcime).

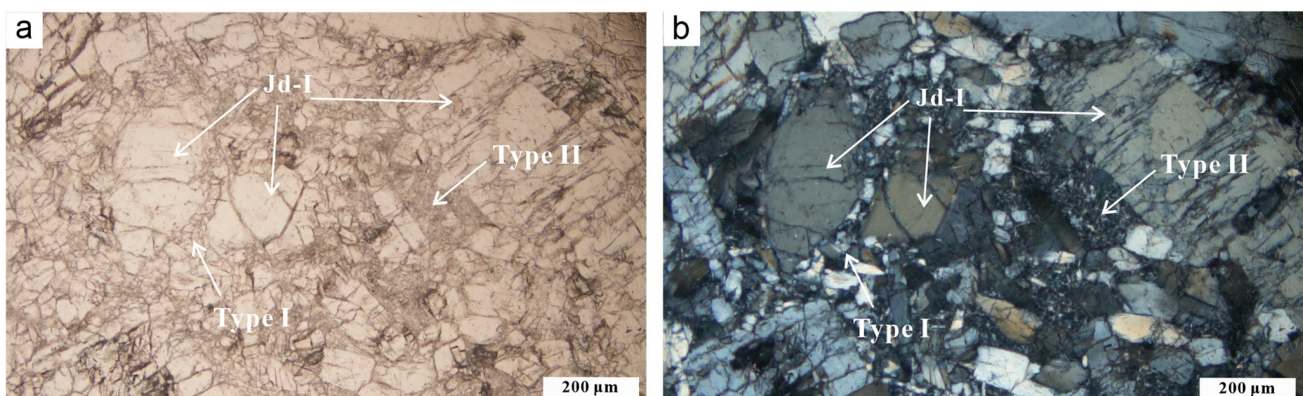


Figure 9. The mixed interstitial textures of the two types can be easily distinguished by grain size ((a) under plane-crossed polarized light and (b) under cross-polarized light).

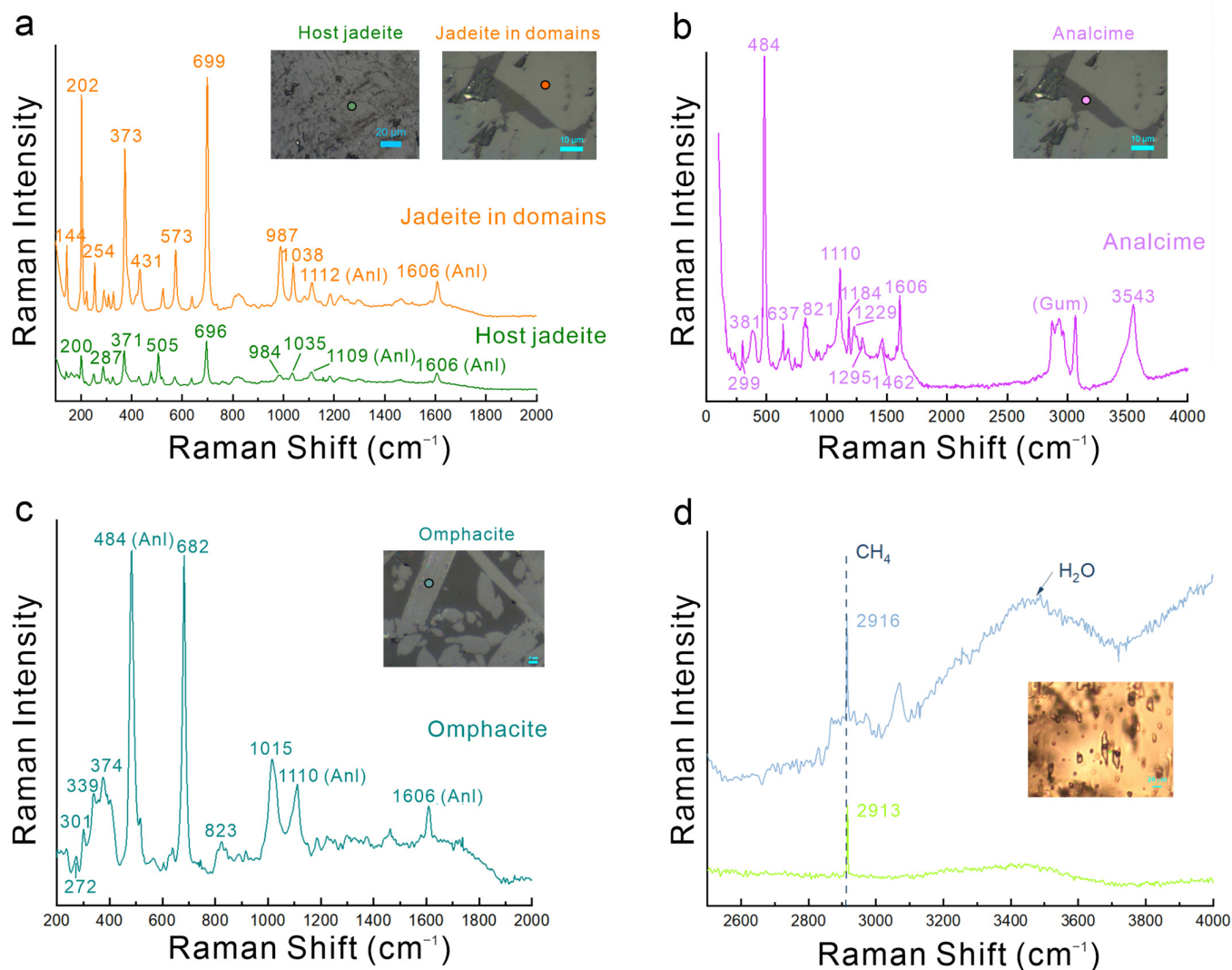


Figure 10. (a) Raman spectra of host jadeite and jadeite in domains. (b,c) Raman spectra reveal that the component of the filling grains in Type II is jadeite (a), analcime, and omphacite. (d) The fluid inclusions show distinct methane peak at $\sim 2916\text{ cm}^{-1}$ and peaks of H₂O (Gum—Canadian gum on the thin section and Anl—analcime).

Jadeite contains 92%–100% Jd with Ca–Mg–Fe pyroxene (Quad) of 0%–8%. Omphacite has 43%–50% Jd, 45%–53% Quad, and up to 6% Ae (Table 1, Figure 11).

Table 1. The chemical compositions of jadeite, omphacite, and analcime in samples.

Test Sections	Host Jadeite		Jadeite in MTDs				Omphacite in MTDs				Analcime	
			Type I		Type II		Type I		Type II			
SiO ₂	60.24	60.84	60.62	60.83	60.78	60.82	58.16	58.35	58.52	58.38	56.97	60.46
TiO ₂	0.04	0.00	0.00	0.01	0.01	0.01	0.21	0.28	0.06	0.18	0.00	0.01
Al ₂ O ₃	22.97	24.87	24.40	25.21	25.20	25.10	11.63	10.41	12.00	11.62	24.99	25.59
FeO ^T	0.24	0.08	0.03	0.00	0.00	0.08	0.76	0.80	0.72	0.64	0.01	0.01
Cr ₂ O ₃	0.01	0.00	0.00	0.00	0.02	0.01	0.01	0.05	0.02	0.00	0.09	0.01
MnO	0.00	0.06	0.00	0.02	0.00	0.00	0.02	0.05	0.05	0.05	0.01	0.07
MgO	1.25	0.26	0.48	0.01	0.00	0.03	8.72	9.53	8.44	8.95	0.05	0.05
CaO	1.84	0.43	0.70	0.15	0.11	0.25	12.31	13.58	12.16	12.67	0.09	0.05

Table 1. Cont.

Test Sections	Host Jadeite		Jadeite in MTDs				Omphacite in MTDs				Analcime	
			Type I		Type II		Type I		Type II			
Na ₂ O	13.38	14.27	14.13	14.44	14.74	14.31	7.16	6.31	7.27	7.04	8.62	6.68
K ₂ O	0.00	0.00	0.01	0.00	0.01	0.01	0.00	0.00	0.01	0.00	0.02	0.00
NiO	0.00	0.04	0.00	0.00	0.00	0.00	0.06	0.01	0.02	0.00	0.00	0.00
Total	99.97	100.85	100.37	100.67	100.87	100.62	99.04	99.37	99.27	99.53	90.85	92.93
Si	2.03	2.02	2.03	2.02	2.02	2.02	2.04	2.05	2.05	2.04	32.79	33.58
Ti	0.00	0.00	0.00	0.00	0.00	0.00	0.01	0.01	0.00	0.01	0.00	0.00
Al ^{IV}	0.00	0.00	0.00	0.00	0.00	0.00	0.00	0.00	0.00	0.00	0.00	0.00
Al ^{VI}	0.91	0.97	0.96	0.99	0.99	0.99	0.48	0.43	0.49	0.48	16.95	16.75
Fe	0.01	0.00	0.00	0.00	0.00	0.00	0.02	0.02	0.02	0.02	0.00	0.00
Mn	0.00	0.00	0.00	0.00	0.00	0.00	0.00	0.00	0.00	0.00	0.00	0.03
Mg	0.06	0.01	0.02	0.00	0.00	0.00	0.46	0.50	0.44	0.47	0.04	0.04
Ca	0.07	0.02	0.03	0.01	0.00	0.01	0.46	0.51	0.46	0.47	0.06	0.03
Na	0.87	0.92	0.92	0.93	0.95	0.92	0.49	0.43	0.49	0.48	9.62	7.19
K	0.00	0.00	0.00	0.00	0.00	0.00	0.00	0.00	0.00	0.00	0.01	0.00
Ni	0.00	0.00	0.00	0.00	0.00	0.00	0.00	0.00	0.00	0.00	0.00	0.00
Cr	0.00	0.00	0.00	0.00	0.00	0.00	0.00	0.00	0.00	0.00	0.04	0.00
Total	3.95	3.95	3.95	3.95	3.96	3.94	3.96	3.95	3.95	3.97	59.51	57.62
Jd	92.30	98.60	97.20	100.00	99.70	99.90	48.60	43.60	50.00	47.80		
Ae	0.00	0.00	0.00	0.00	0.00	0.00	6.00	0.00	0.00	0.00		
Quad	7.70	1.40	2.80	0.00	0.30	0.10	45.40	56.40	50.00	52.20		
Name	Jd	Jd	Jd	Jd	Jd	Jd	Omp	Omp	Omp	Omp	Anl	Anl

Note: The cations were calculated with 6 O as standards in pyroxenes and 96 O in analcime (Fe^O: Total iron as FeO. Al^{IV}: Tetrahedral coordination. Al^{VI}: Octahedral coordination. Jd—Jadeite, Omp—omphacite, Anl—analcime, Ae—aegirine, and Quad: Ca–Mg–Fe pyroxene).

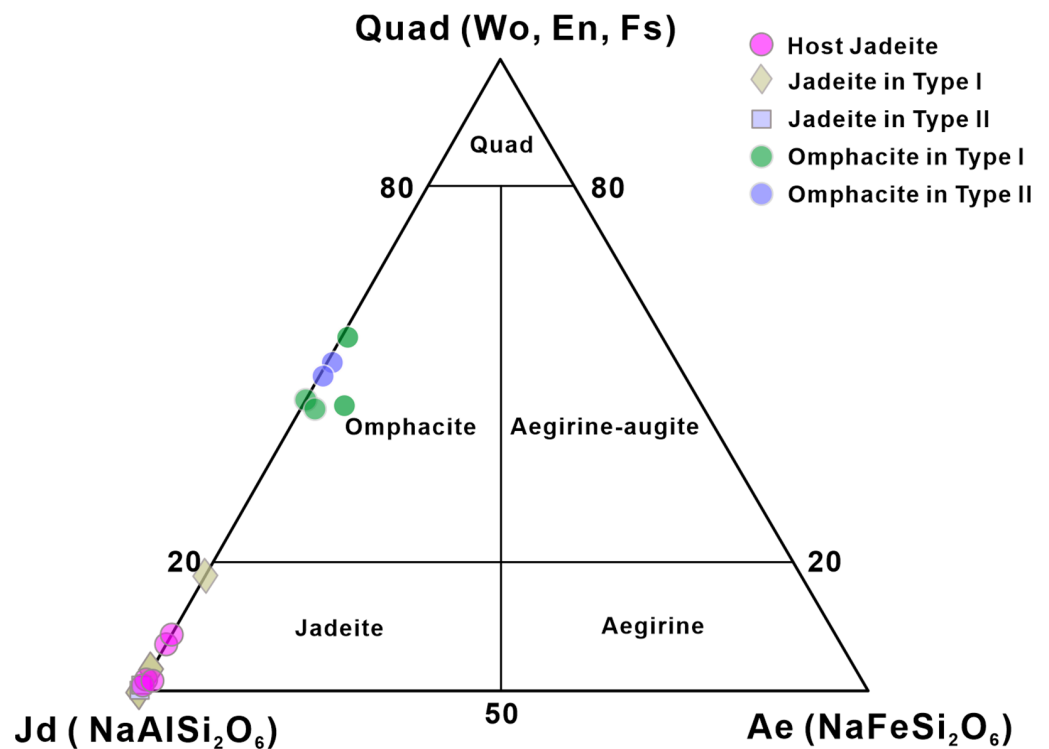


Figure 11. Kazakhstan jadeiteite Quad–Jd–Ae triple diagram (modified from [44]).

5. Discussion

5.1. The Formation of Interspaces within the Coarser Hosts

The interspaces among the coarser grains provide space for the crystallization of the later fluid and are, therefore, essential for the formation of the interstitial textures. According to this observation, a hypothesis for the earlier stage crystallization process was proposed (Figure 12).

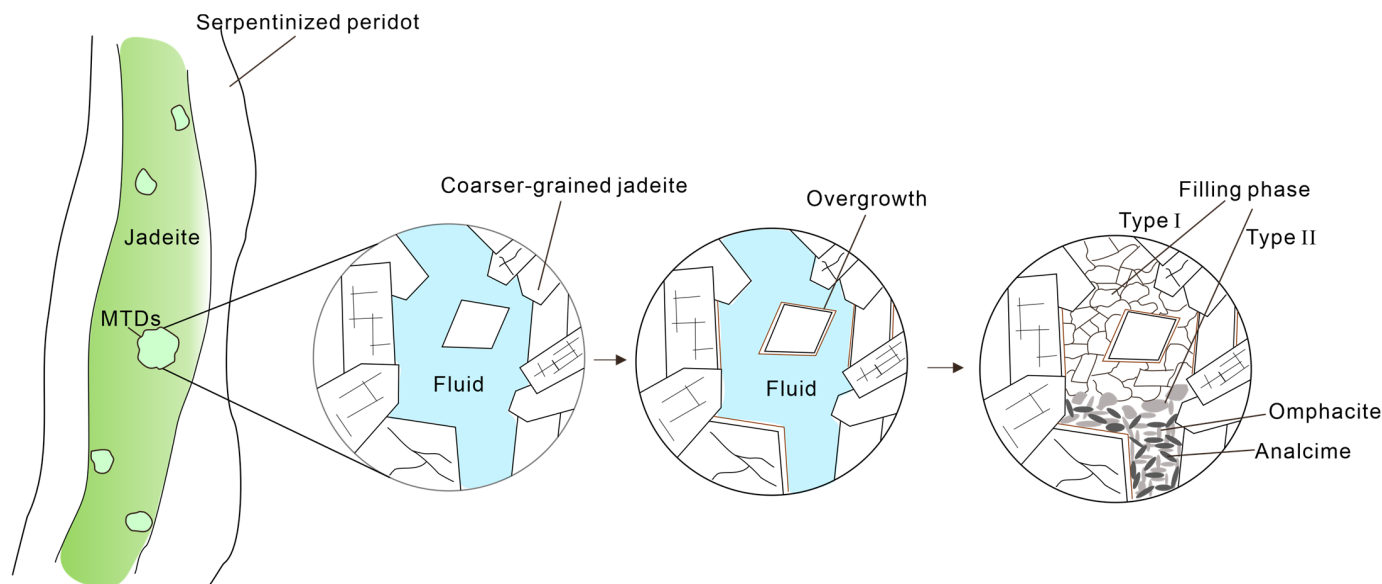


Figure 12. Schematic diagram of the formation process of interstitial textures (from left to right): (1) fluid enters serpentinized peridotite cracks and crystallizes into jadeites; (2) coarse-grained jadeites stop growing and form interspaces and interspaces; (3) relict or later-stage hydrothermal fluids enter the interspaces and form Type I filling grains in the respectively larger space; (4) crystallization continues in the narrow space to form anhedral Type II filling grains, and then analcime forms in crystal interstices, fractures, and hollows.

The majority of the jadeite found in Kazakhstan is P-type. The Na–Al–Si-rich fluid penetrates and precipitates in the fractures of serpentinized peridotite or low-temperature, high-pressure metamorphic rocks [21]. It is hypothesized that the formation space for host jadeite was sufficient, or the fluid was insufficient as interspaces among the coarser grain exist. Only a few crystal nuclei can form when combined with the low undercooling rate and poor fluid nucleation rate [45,46]. The fluid then steadily crystallized, generating coarser jadeite grains. After the crystals reached a specific size, however, due to sufficient space or insufficient fluid supply, the crystallization paused, leaving interspace among the existing jadeite crystals [46].

Such a pause might end if fluids are resupplied. A later stage of fluid supply would lead to the overgrowth of some coarser grains and the formation of the MTDs as the fluids enter the interspace.

After the coarse grains grow, the rocks may go through brittle deformation and form a lot of cataclasis. These cataclases provide the necessary channels for fluids to enter and form the domains.

5.2. The Formation of the Domains

According to mineral morphology and contact relationship observations, finer grains formed later than euhedral coarser-grained crystals. In addition, the fluid inclusions containing methane and water suggest that both hosts and MTDs are P-type and formed in an extremely reductive environment. After the interspaces formed, the fluid crystallized along the outlines of the host jadeite, forming the overgrowths. Meanwhile, the filling

crystals might start to grow. According to the crystal growth theory, small crystals are more likely to form when supersaturation is high or the crystallization speed is fast [47], and viscosity and volatile substances affect the nucleation rate of crystals. The lower the viscosity, the easier the nucleation; the higher the volatile contents, the more difficult the nucleation [47,48]. The morphology of the filling crystals suggests that they had a high nucleation rate. During the formation of the interstitial textures, it is possible that the environment of crystallization changed rapidly, thus resulting in numerous tiny crystals [48,49]. Furthermore, as there was not enough room for so many crystal nuclei to crystallize, subhedral to anhedral pyroxenes occurred.

The majority of the analcime in Type II interstitial textures was found in the cracks of jadeite and omphacite, which was determined to be of a later phase. Thus, it is proposed that jadeite might undergo a hydration reaction to form analcime [1,18], and the following reaction might occur:



The analcime might form from the fluids, as in the samples, because analcimes do not show obvious replacement features.

The presence of two types of mixed textures (Figure 9) implies that the crystallization process is probably as follows: First, the coarser-grained jadeite precipitated from fluid and interspaces were left among them. Afterwards, the two types of interstitial textures began to crystallize. Since the grain size of Type I is much larger than that of Type II, it is assumed that Type I crystallized earlier than Type II in the mixed textures. After the formation of Type I, relict space still remained, and the fluid then continued to be batched in the remaining narrow space under a suitable environment, forming finer anhedral finer grains (Type II) (Figure 12).

5.3. Significance of Interspace Domains among the Coarser Hosts

Similar phases have been reported worldwide, but all different from those in Kazakhstan (Table 2). In Myanmar, anhedral hyalophane and hydrated barium aluminum silicate occur interstitially in jadeite and amphibole [23]. In Guatemala, mica, ablite, and analcime occur as interstitial phases and inclusions in the jadeite matrix [50,51]. In Japan, the tiny euhedral jadeite crystals are interstitially filled by grossular, natrolite, matsubaraite, and barian feldspars [6,22,52–54]. In Cuba, albite crosscuts massive jadeite to form lighter green veins associated with omphacite; anhedral biotite occurs in the jadeite matrix, and allanite in contact with epidote is associated with chlorite at the interstitial textural position [55]. In Dominica, albite is interstitial in the jadeite matrix [56]. In the Polar Urals, omphacite is vein-like in jadeite, and clinocllore is seen as euhedral flakes in amphibole [57]. Phengite and analcime in pre-Columbian jadeitite artifacts occur as interstitial anhedral monominerals in jadeite [58]. However, none of those have been found in relation to jadeitite's local transparency of jadeitite.

The interstitial textures are very common in Kazakhstan and are visible to the naked eye. These textures have a significant effect on the local transparency of jadeitite, and other sources do not have this effect. Moreover, the interstitial texture in Kazakhstan is unique in size, mineral assemblage, and microstructure.

The main sources of jadeitite supply into the Chinese market now are Myanmar and Guatemala. Shi et al. [27] discovered that dynamic metamorphism has significant impacts on the transparency of jadeite jade. Large-scale metamorphism and recrystallization can homogenize the chemical composition of jadeite, improve grain boundary migration (GBM), shrink the size of crystal grains, and enhance the preferred orientation (mainly the shape preferred orientation (SPO) and crystal preferred orientation (CPO)). Furthermore, the recovery textures (foam texture) formed by recrystallization can greatly improve the transparency of jadeitite as well, making it appear as an icy or glassy species [27,59]. Shearing may improve the local transparency of jadeitite as well. Jadeitites from Myanmar and Guatemala both experienced shearing. Some jadeite grains around the micro shear zones are finer and highly preferred due to being oriented SPO and CPO under a

microscope. Fine-grained jadeitite causes the light transmission path to approach a straight line, reducing light loss and forming high-transparency jadeitite [60–64]. When comparing Kazakhstan jadeitite with that from Myanmar and Guatemala, the most noteworthy feature is that only the domains are more transparent than the matrix, which can be used as a key identifying feature of Kazakhstan jadeitite.

Table 2. Interstitial phases occurring in jadeitite from different localities and their mineral assemblages.

locality	mineral assemblages and appearance in jadeitite
Myanmar [23]	hyalophane and hydrated barium aluminum silicate: sometimes crosscutting the jadeite
Guatemala [1,50,51]	albite, analcime, white-to-tan mica(s): appearing as interstitial phase or inclusions, micrometer to multi-millimeter in size
Osayama, Japan [22]	grossular: appearing as interstitial phase or inclusions
Itoigawa-Ohmi, Japan [6,52–54]	natrolite, matsubaraitite, Sr-bearing minerals and barian feldspars: occurring as aggregates and hollow crystals with tiny size
Eastern Cuba [55]	albite: crosscutting massive jadeite, together with omphacite results in lighter green veins.
Dominican Republic [56]	albite: showing anhedral monomineralic grains
Polar Urals [57]	omphacite, jadeite, clinocllore: pyroxenes are vien-like and clinocllore are visible as euhedral flakes
Pre-Columbian jadeitite artifacts from Caribbean [58]	phengite: coarser than surrounding minerals

6. Conclusions

In this study, interstitial textures were found to commonly occur within the coarse-grained textures of Kazakhstan jadeitite.

The interstitial textures have distinct boundaries and higher transparency than the matrix to the naked eye. Within the interstitial textures, subhedral to anhedral jadeite grains mainly form Type I MTDs, while euhedral to subhedral jadeite and omphacite, and anhedral analcime form Type II MTDs. The finer grains in the interstitial textures are suggested to be related to the improvements in partial macro-transparency.

The interstitial textures are more likely to form under different temperatures, pressures, and/or fluid conditions from the coarse-grained textures.

The interstitial textures in Kazakhstan are easily recognizable to the naked eye and have a significantly higher transparency than the coarse-grained jadeitite matrix, which makes it unique. The macroscopic MTDs have not yet been found in jadeitites from other localities, so exclusive origin significance, together with the mineral assemblage and textures, can help distinguish Kazakhstan jadeitite from other jadeitites both with the naked eye and via microscopic observation.

Author Contributions: Conceptualization, J.W. and G.S.; methodology, J.W.; software, J.W.; validation, J.W. and B.X.; formal analysis, J.W., B.X. and G.S.; investigation, J.W., B.X., T.L. and G.S.; resources, G.S., T.L. and J.Z.; writing—original draft preparation, J.W. and G.S.; writing—review and editing, J.W., B.X. and G.S.; visualization, J.W.; supervision, G.S.; project administration, G.S.; funding acquisition, G.S. All authors have read and agreed to the published version of the manuscript.

Funding: This work was supported by the National Natural Science Foundation of China (Grant/Award Numbers: 42273044) and the National Key R&D Program of China (Grant/Award Numbers: 2022YFC2903302).

Data Availability Statement: Data are contained within the article. Data available on request from the authors.

Acknowledgments: Thanks to Shih, M.Y., Zhang, L.J., Wu, M.K., Han, J.Y. and Wu, X.R. at CUGB for their analytic supports. Thanks to Chen, Z.Y. for the EPM analyses support. Thanks to Zhang, X.Y. for other analyses support. We are grateful to the editor, Fillp Kostic, for his valuable comments and suggestions, to Harlow, G.E. and one anonymous reviewer for their helpful and constructive comments.

Conflicts of Interest: The authors declare that there are no conflict of interest.

References

1. Harlow, G.E. Jadeitites, albitites and related rocks from the Motagua Fault Zone, Guatemala. *J. Metamorph. Geol.* **1994**, *12*, 49–68. [[CrossRef](#)]
2. Harlow, G.E.; Sisson, V.B.; Sorensen, S.S. Jadeitite from Guatemala: New observations and distinctions among multiple occurrences. *Geol. Acta* **2011**, *9*, 363. [[CrossRef](#)]
3. Flores, K.E.; Martens, U.C.; Harlow, G.E.; Brueckner, H.K.; Pearson, N.J. Jadeitite formed during subduction: In situ zircon geochronology constraints from two different tectonic events within the Guatemala Suture Zone. *Earth Planet. Sci. Lett.* **2013**, *371–372*, 67–81. [[CrossRef](#)]
4. Garcia-Casco, A.; Rodriguez Vega, A.; Cardenas Parraga, J.; Iturralde-Vinent, M.A.; Lazaro, C.; Blanco Quintero, I.; Rojas-Agramonte, Y.; Kroener, A.; Nunez Cambra, K.; Millan, G.; et al. A new jadeitite jade locality (Sierra del Convento, Cuba): First report and some petrological and archeological implications. *Contrib. Mineral. Petrol.* **2009**, *158*, 1–16. [[CrossRef](#)]
5. Krebs, M.; Schertl, H.P.; Maresch, W.V.; Draper, G. Mass flow in serpentinite-hosted subduction channels: P-T-t path patterns of metamorphic blocks in the Rio San Juan melange (Dominican Republic). *J. Asian Earth Sci.* **2011**, *42*, 569–595. [[CrossRef](#)]
6. Miyajima, H.; Matsubara, S.; Miyawaki, R.; Ito, K. Itoigawaite, a new mineral, the Sr analogue of lawsonite, in jadeitite from the Itoigawa-Ohmi district, central Japan. *Mineral. Mag.* **1999**, *63*, 909–916. [[CrossRef](#)]
7. Tsujimori, T. Omphacite-diopside vein in an omphacite block from the Osayama serpentinite melange, Sangun-Renge metamorphic belt, southwestern Japan. *Mineral. Mag.* **1997**, *61*, 845–852. [[CrossRef](#)]
8. Tsujimori, T.; Liou, J.G. Significance of the Ca-Na pyroxene-lawsonite-chlorite assemblage in blueschist-facies metabasalts: An example from the rengo metamorphic rocks, Southwest Japan. *Int. Geol. Rev.* **2007**, *49*, 416–430. [[CrossRef](#)]
9. Shigeno, M.; Mori, Y.; Nishiyama, T. Reaction microtextures in jadeitites from the Nishisonogi metamorphic rocks, Kyushu, Japan. *J. Mineral. Petrol.* **2005**, *100*, 237–246. [[CrossRef](#)]
10. Hirajima, T. Jadeite and jadeitite-bearing rock in the Sanbagawa and the Kamuikotan belts, Japan: A review. *J. Mineral. Petrol.* **2017**, *112*, 237–246. [[CrossRef](#)]
11. Coleman, R.G. Jadeite Deposits of the Clear Creek Area, New Idria District, San Benito County, California. *J. Petrol.* **1961**, *2*, 209–247. [[CrossRef](#)]
12. Banno, S.; Shibakusa, H.; Enami, M.; Wang, C.L.; Ernst, W.G. Chemical fine structure of Franciscan jadeitic pyroxene from Ward Creek, Cazadero area, California. *Am. Mineral.* **2000**, *85*, 1795–1798. [[CrossRef](#)]
13. Harlow, G.E.; Summerhayes, G.R.; Davies, H.L.; Matisoo-Smith, L. A jade gouge from Emirau Island, Papua New Guinea (Early Lapita context, 3300 BP): A unique jadeitite. *Eur. J. Mineral.* **2012**, *24*, 391–399. [[CrossRef](#)]
14. Fu, B.; Paul, B.; Cliff, J.; Broecker, M.; Bulle, F. O-Hf isotope constraints on the origin of zircon in high-pressure melange blocks and associated matrix rocks from Tinos and Syros, Greece. *Eur. J. Mineral.* **2012**, *24*, 277–287. [[CrossRef](#)]
15. Compagnoni, R.; Rolfo, F.; Groppo, C.; Hirajima, T.; Turello, R. Geological map of the ultra-high pressure Brossasco-Isasca unit (Western Alps, Italy). *J. Maps* **2012**, *8*, 465–472. [[CrossRef](#)]
16. Oberhansli, R.; Bousquet, R.; Moazzzen, M.; Arvin, M. The field of stability of blue jadeite: A new occurrence of jadeitite at Sorkhan, Iran, as a case study. *Can. Mineral.* **2007**, *45*, 1501–1509. [[CrossRef](#)]
17. Shi, G.H.; Cui, W.Y.; Liu, J.; Yu, H.X. Petrology of jadeite-bearing serpentinitized peridotite and its country rocks from Northwestern Myanmar (Burma). *Acta Petrol.* **2001**, *17*, 483–490.
18. Shi, G.H.; Harlow, G.E.; Wang, J.; Wang, J.; Enoch, N.G.; Wang, X.; Cao, S.M.; Cui, W.Y. Mineralogy of jadeitite and related rocks from Myanmar: A review with new data. *Eur. J. Mineral.* **2012**, *24*, 345–370. [[CrossRef](#)]
19. Dobretsov, N.L.; Buslov, M.M. Serpentinic mélanges associated with UP and UHP rocks in Central Asia. *Int. Geol. Rev.* **2004**, *46*, 957–980. [[CrossRef](#)]
20. Krzemnicki, M.; Franz, L.; Ernst, K.; Capitani, C.; Harlow, G.; Kouznetsov, N. Kosmochlor-bearing jadeite rocks from Kenterlau-Itmurundy (Lake Balkhash, Kazakhstan). In Proceedings of the International Gemmological Conference, Windhoek, Namibia, 11–15 October 2017.
21. Harlow, G.E.; Tsujimori, T.; Sorensen, S.S. Jadeitites and Plate Tectonics. *Annu. Rev. Earth Planet. Sci.* **2015**, *43*, 105–138. [[CrossRef](#)]
22. Tsujimori, T.; Harlow, G.E. Petrogenetic relationships between jadeitite and associated high-pressure and low-temperature metamorphic rocks in worldwide jadeitite localities: A review. *Eur. J. Mineral.* **2012**, *24*, 371–390. [[CrossRef](#)]
23. Shi, G.H.; Jiang, N.; Wang, Y.W.; Zhao, X.; Wang, X.; Li, G.W.; Ng, E.; Cui, W.Y. Ba minerals in clinopyroxene rocks from the Myanmar jadeitite area: Implications for Ba recycling in subduction zones. *Eur. J. Mineral.* **2010**, *22*, 199–214. [[CrossRef](#)]
24. Harlow, G.E.; Flores, K.E.; Marschall, H.R. Fluid-mediated mass transfer from a paleosubduction channel to its mantle wedge: Evidence from jadeitite and related rocks from the Guatemala Suture Zone. *Lithos* **2016**, *258–259*, 15–36. [[CrossRef](#)]

25. Ng, Y.N.; Shi, G.H.; Santosh, M. Titanite-bearing omphacite from the Jade Tract, Myanmar: Interpretation from mineral and trace element compositions. *J. Asian Earth Sci.* **2016**, *117*, 1–12. [[CrossRef](#)]
26. Xing, B.Q.; Shi, G.H.; Long, T.; Shih, M.Y. Locality determination of inky black omphacite jades from Myanmar and Guatemala by nondestructive analysis. *J. Raman Spectrosc.* **2022**, *53*, 2009–2018. [[CrossRef](#)]
27. Shi, G.H.; Wang, X.; Chu, B.B.; Cui, W.Y. Jadeite jade from Myanmar: Its texture and gemmological implications. *J. Gemol.* **2009**, *31*, 185–195. [[CrossRef](#)]
28. Orzol, J.; Trepmann, C.A.; Stockhert, B.; Shi, G. Critical shear stress for mechanical twinning of jadeite—An experimental study. *Tectonophysics* **2003**, *372*, 135–145. [[CrossRef](#)]
29. Dobretsov, N.; Berzin, N.; Buslov, M. Opening and Tectonic Evolution of the Paleo-Asian Ocean. *Int. Geol. Rev.* **1995**, *37*, 335–360. [[CrossRef](#)]
30. Kroener, A.; Windley, B.F.; Badarch, G.; Tomurtogoo, O.; Hegner, E.; Jahn, B.M.; Gruschka, S.; Khain, E.V.; Demoux, A.; Wingate, M.T.D. Accretionary growth and crust formation in the Central Asian Orogenic Belt and comparison with the Arabian-Nubian shield. In Proceedings of the 17th International Conference on Basement Tectonics, Oak Ridge, TN, USA, 27 June–1 July 2004; pp. 181–209.
31. Windley, B.F.; Alexeiev, D.; Xiao, W.; Kröner, A.; Badarch, G. Tectonic models for accretion of the Central Asian Orogenic Belt. *J. Geol. Soc.* **2007**, *164*, 31–47. [[CrossRef](#)]
32. Kröner, A.; Hegner, E.; Lehmann, B.; Heinhorst, J.; Wingate, M.T.D.; Liu, D.Y.; Ermelov, P. Palaeozoic arc magmatism in the Central Asian Orogenic Belt of Kazakhstan: SHRIMP zircon ages and whole-rock Nd isotopic systematics. *J. Asian Earth Sci.* **2008**, *32*, 118–130. [[CrossRef](#)]
33. Filippova, I.B.; Bushi, V.A.; Didenko, A.N. Middle Paleozoic subduction belts: The leading factor in the formation of the Central Asian fold-and-thrust belt. *Russ. J. Earth Sci.* **2001**, *3*, 405–426. [[CrossRef](#)]
34. Li, G.M.; Qin, K.Z.; Li, J.X. Study on geological and metallogenic background of porphyry copper deposits around Balkhash in Kazakhstan. *Acta Petrol. Sin.* **2008**, *24*, 2679–2700.
35. Liang, X.; Zhang, J.Q.; Lu, J.; Wang, L.X.; Li, Y.Q.; Wu, W.Z.; Li, Q.; Wang, Y.Q. Mineralogical characteristics of the Itemurun jadeite from Kazakhstan. *Acta Mineral. Sin.* **2020**, *40*, 155–164. [[CrossRef](#)]
36. Sorensen, S.; Harlow, G.E.; Rumble, D., III. The origin of jadeite-forming subduction-zone fluids: CL-guided SIMS oxygen-isotope and trace-element evidence. *Am. Mineral.* **2006**, *91*, 979–996. [[CrossRef](#)]
37. Harlow, G.E.; Sorensen, S. Jade (Nephrite and Jadeite) and Serpentine: Metasomatic Connections. *Int. Geol. Rev.* **2005**, *47*, 113–146. [[CrossRef](#)]
38. Kovalenko, I.; Aerov, G.; Bagrova, Z. Geological and structural conditions localizing ornamental stone occurrence in the ophiolites of Itmurunda zone, Kazakhstan. In *Circum-Pacific Ophiolites*; Ishiwatari, A., Malpas, J., Ishizuka, H., Eds.; VSP: Utrecht, The Netherlands, 1994; pp. 255–262.
39. Safonova, I.Y.; Perfilova, A.A.; Obut, O.T.; Savinsky, I.A.; Chyorny, R.I.; Petrenko, N.A.; Gurova, A.V.; Kotler, P.D.; Khromykh, S.V.; Krivonogov, S.K.; et al. The Itmurundy Accretionary Complex, Northern Balkhash Area: Geological Structure, Stratigraphy and Tectonic Origin. *Russ. J. Pac. Geol.* **2019**, *13*, 283–296. [[CrossRef](#)]
40. Safonova, I.; Savinskiy, I.; Perfilova, A.; Gurova, A.; Maruyama, S.; Tsujimori, T. The Itmurundy Pacific-type orogenic belt in northern Balkhash, central Kazakhstan: Revisited plus first U–Pb age, geochemical and Nd isotope data from igneous rocks. *Gondwana Res.* **2020**, *79*, 49–69. [[CrossRef](#)]
41. Zhylykaidarov, A. Conodonts from Ordovician ophiolites of central Kazakhstan. *Acta Palaeontol. Pol.* **1998**, *43*, 53–68.
42. Zhang, X.Y.; Shi, G.H.; Li, G.W.; Li, X. Weathered Cortex of Eluvial-Deluvial Jadeite Jade from Myanmar: Its Features, Formation Mechanism, and Implications. *Minerals* **2022**, *12*, 797. [[CrossRef](#)]
43. Dobretsov, N.L.; Ponomareva, L.G. Comparative characteristics of jadeite and associated rocks from Polar Ural and Near-Balkhash Region. *Acad. Sci. USSR (Sib. Branch) Tr. Inst. Geol. Geophys.* **1965**, *31*, 178–243.
44. Morimoto, N.; Fabries, J.; Ferguson, A.K.; Ginzburg, I.V.; Ross, M.; Seifert, F.A.; Zussman, J.; Aoki, K.; Gottardi, G. Nomenclature of Pyroxenes. *Bull. De Mineral.* **1988**, *111*, 535–550. [[CrossRef](#)]
45. Fu, H.Y.; Sheng, J.; Ling, L. A new perspective of inorganic crystallization: Nonclassical nucleation and growth. *Sci. Bull.* **2021**, *66*, 4256–4267.
46. Li, G.H.; Han, L.; Fang, Q. Theory and application of crystal structure controlling crystal morphology. *J. Artif. Cryst.* **2005**, *34*, 546–549. [[CrossRef](#)]
47. Hao, B.H.; Huang, J.H. A review of research on crystal growth mechanism. *J. Beijing Inst. Petro-Chem. Technol.* **2006**, *14*, 58–64.
48. Christoph, H.; Matthias, K. Determination of Crystal Growth Rates in Multi-Component Solutions. *Crystals* **2022**, *12*, 1568.
49. Feigelson, R.S. Crystal growth History: Theory and melt growth processes. *J. Cryst. Growth* **2022**, *594*, 126800. [[CrossRef](#)]
50. Harlow, G.E. Crystal chemistry of barium enrichment in micas from metasomatized inclusions in serpentinite, Motagua Fault Zone, Guatemala. *Eur. J. Mineral.* **1995**, *7*, 775–790. [[CrossRef](#)]
51. Martens, U.; Solari, L.; Sisson, V.; Harlow, G.; de León, R.T.; Ligorria, J.P.; Tsujimori, T.; Ortega, F.; Brueckner, H.; Giunta, G.; et al. High-Pressure Belts of Central Guatemala: The Motagua Suture and the Chuacús Complex. In *Field Trip Guide 1st Field Workshop of IGCP 546 “Subduction Zones of the Caribbean”*; Workshop of IGCP 546, Unesco: Stanford, CA, USA, 2007.
52. Miyajima, H.; Miyawaki, R.; Ito, K. Matsubaraite, Sr₄Ti₅(Si₂O₇)₂O₈, a new mineral, the Sr-Ti analogue of perrierite in jadeite from the Itoigawa-Ohmi district, Niigata Prefecture, Japan. *Eur. J. Mineral.* **2002**, *14*, 1119–1128. [[CrossRef](#)]

53. Morishita, T.; Arai, S.; Ishida, Y. Trace element compositions of jadeite (+omphacite) in jadeitites from the Itoigawa-Ohmi district, Japan: Implications for fluid processes in subduction zones. *Island Arc*. **2007**, *16*, 40–56. [[CrossRef](#)]
54. Miyajima, H. Jadeitite from Itoigawa, Niigata Prefecture, central Japan. *J. Mineral. Petrol. Sci.* **2017**, *112*, 227–236. [[CrossRef](#)]
55. Cárdenas-Párraga, J.; García-Casco, A.; Harlow, G.E.; Blanco-Quintero, I.F.; Agramonte, Y.R.; Kröner, A. Hydrothermal origin and age of jadeitites from Sierra del Convento Mélange (Eastern Cuba). *Eur. J. Mineral.* **2012**, *24*, 313–331. [[CrossRef](#)]
56. Kawamoto, T.; Hertwig, A.; Schertl, H.-P.; Maresch, W.V. Fluid inclusions in jadeitite and jadeite-rich rock from serpentinite mélanges in northern Hispaniola: Trapped ambient fluids in a cold subduction channel. *Lithos* **2018**, *308–309*, 227–241. [[CrossRef](#)]
57. Angiboust, S.; Glodny, J.; Cambeses, A.; Raimondo, T.; Monié, P.; Popov, M.; Garcia-Casco, A. Drainage of subduction interface fluids into the forearc mantle evidenced by a pristine jadeitite network (Polar Urals). *J. Metamorph. Geol.* **2020**, *39*, 473–500. [[CrossRef](#)]
58. Garcia-Casco, A.; Knippenberg, S.; Rodríguez Ramos, R.; Harlow, G.E.; Hofman, C.; Pomo, J.C.; Blanco-Quintero, I.F. Pre-Columbian jadeitite artifacts from the Golden Rock Site, St. Eustatius, Lesser Antilles, with special reference to jadeitite artifacts from Elliot's, Antigua: Implications for potential source regions and long-distance exchange networks in the Greater Caribbean. *J. Archaeol. Sci.* **2013**, *40*, 3153–3169. [[CrossRef](#)]
59. Wang, J.; Shi, G.H.; Wang, J. Structure and microstructure of Myanmar albite jade: Gemmological significance. In Proceedings of the 2009 China Jewelry Academic Exchange Conference, Beijing, China, 3 November 2009; pp. 229–235.
60. Wang, L.S.; Zhang, H.H.; Liu, J.Y.; Wang, L.S.; Ouyang, Q.M.; Liu, D.M.; Liu, W. Mineral Component and Genesis of High-Grade Green Jadeite Jade from Guatemala. *Gems Gemol.* **2022**, *24*, 11–30. [[CrossRef](#)]
61. Yi, X.; Shi, G.H.; He, M.Y. Jadeitized omphacitite from Myanmar jadeite area. *Acta Petrol. Sin.* **2006**, *22*, 971–976.
62. Zhang, Y.; Shi, G.H. Origin of Blue-Water Jadeite Jades from Myanmar and Guatemala: Differentiation by Non-Destructive Spectroscopic Techniques. *Crystals* **2022**, *12*, 1448. [[CrossRef](#)]
63. Xing, B.Q.; Shi, G.H.; Zhang, J.H.; Long, C.; Zhang, Y.; He, L.Y.; Hu, R.J. Mineralogical characteristics of Guatemalan jadeite gemstones and their comparison with Myanmar jadeite. *Geosciences* **2021**, *35*, 1769–1788.
64. Zou, Y.; Liang, Y.W.; Liu, Y.D.; Wang, D.; Yang, L. Chemical composition and structural characteristics of jadeite minerals from Myanmar, Kazakhstan and Russia. *Silic. Bull.* **2017**, *36*, 144–152. [[CrossRef](#)]

Disclaimer/Publisher's Note: The statements, opinions and data contained in all publications are solely those of the individual author(s) and contributor(s) and not of MDPI and/or the editor(s). MDPI and/or the editor(s) disclaim responsibility for any injury to people or property resulting from any ideas, methods, instructions or products referred to in the content.